AIP Journal of Applied Physics

Radiative decay rate of excitons in square quantum wells: Microscopic modeling and experiment

E. S. Khramtsov, P. A. Belov, P. S. Grigoryev, I. V. Ignatiev, S. Yu. Verbin, Yu. P. Efimov, S. A. Eliseev, V. A. Lovtcius, V. V. Petrov, and S. L. Yakovlev

Citation: Journal of Applied Physics **119**, 184301 (2016); doi: 10.1063/1.4948664
View online: http://dx.doi.org/10.1063/1.4948664
View Table of Contents: http://scitation.aip.org/content/aip/journal/jap/119/18?ver=pdfcov
Published by the AIP Publishing

Radiative decay rate of excitons in square quantum wells: Microscopic modeling and experiment

E. S. Khramtsov,[1] P. A. Belov,[2,a)] P. S. Grigoryev,[1] I. V. Ignatiev,[1] S. Yu. Verbin,[1] Yu. P. Efimov,[2] S. A. Eliseev,[2] V. A. Lovtcius,[2] V. V. Petrov,[2] and S. L. Yakovlev[2]
[1]*Spin Optics Laboratory, St. Petersburg State University, Ulyanovskaya 1, 198504 St. Petersburg, Russia*
[2]*Department of Physics, St. Petersburg State University, Ulyanovskaya 1, 198504 St. Petersburg, Russia*

(Received 11 December 2015; accepted 23 April 2016; published online 9 May 2016)

The binding energy and the corresponding wave function of excitons in GaAs-based finite square quantum wells (QWs) are calculated by the direct numerical solution of the three-dimensional Schrödinger equation. The precise results for the lowest exciton state are obtained by the Hamiltonian discretization using the high-order finite-difference scheme. The microscopic calculations are compared with the results obtained by the standard variational approach. The exciton binding energies found by two methods coincide within 0.1 meV for the wide range of QW widths. The radiative decay rate is calculated for QWs of various widths using the exciton wave functions obtained by direct and variational methods. The radiative decay rates are confronted with the experimental data measured for high-quality GaAs/AlGaAs and InGaAs/GaAs QW heterostructures grown by molecular beam epitaxy. The calculated and measured values are in good agreement, though slight differences with earlier calculations of the radiative decay rate are observed. *Published by AIP Publishing*. [http://dx.doi.org/10.1063/1.4948664]

I. INTRODUCTION

The optical properties of semiconductor heterostructures have been of growing interest during the last decades due to various applications, e.g., light-emitting diodes and semiconductor lasers.[1–3] Modern epitaxial techniques allow one to grow heterostructures with quantum wells (QWs) and superlattices where the quantum confinement of carriers strongly modifies their energy spectrum. The optical properties of such structures significantly depend on the structure design, layer composition, layer potential profile, etc. This variety of the structural properties is a basis for proposals of new devices like an excitonic transistor,[4] an exciton-polariton router,[5,6] and a transistor switch.[7]

A particular role of excitons in the optical transitions has been understood since their discovery in a bulk semiconductor in 1952.[8] One of the important characteristics of an exciton is the binding energy caused by the Coulomb interaction of the electron and the hole.[9–13] In many bulk semiconductors, this energy is relatively small, typically lower than the lattice vibration energy at room temperature. It is much larger in the wide bandgap semiconductors like GaN and ZnO so that the exciton effects dominate in optical transitions even at room temperature.[14,15] In the semiconductor heterostructures with QWs, the binding energy can significantly increase further.[9]

Together with the binding energy, the radiative properties of an exciton are characterized by another important parameter, the radiative decay rate[11] or the oscillator strength,[16] which is defined by the exciton-light coupling. Since the discovery of the giant exciton oscillator strength (the Rashba effect[17]), the exciton states and exciton-light coupling have been drawing much attention.[18–20] Recent developments of the microcavities[21,22] open up new frontiers for controlling the exciton-light coupling efficiency.

A precise experimental determination of the exciton binding energy is usually complicated by inhomogeneity of the exciton ensemble in heterostructures due to defects and roughness of the interfaces.[12,13] The experimental study of exciton-light coupling is also a nontrivial problem. The coupling gives rise to an energy shift and a radiative broadening of exciton lines,[11] which can be, in principle, measured using, e.g., the steady-state reflectance spectroscopy.[23–25] This method, however, is applicable only for the high-quality heterostructures when the non-radiative broadening does not dominate over the radiative one. Another approach is the time-resolved spectroscopy using photoluminescence kinetics, pump-probe, or four-wave mixing methods for the determination of the radiative decay time.[21,26–29] Similar problems appear in this approach if the quality of the heterostructure is not high enough.

The theoretical modeling of the exciton in a bulk semiconductor is usually carried out in the framework of the envelope function approximation (EFA), which, in the simplest case, leads to the hydrogen model.[16] In this model, the motion of an exciton as a whole and the relative motion of the electron and the hole are separated. This leads to two independent Schrödinger equations (SEs) for the center-of-mass and intrinsic motions. The latter one is similar to the SE for a hydrogen atom and can be analytically reduced to the one-dimensional problem. The hydrogen model becomes unsuitable for semiconductors with a degenerate valence band.[30] In this case, the Luttinger Hamiltonian,[31] which couples the center-of-mass and intrinsic electron-hole motions, is more appropriate. As a result, the variables of the exciton SE cannot be separated and one has to consider the

a)Electronic mail: pavelbelov@gmail.com

multi-dimensional SE. A study of the exciton in a QW meets further complications of the problem. Even when only the diagonal part of the Luttinger Hamiltonian is included in the problem, the presence of the QW potential requires one to consider at least the three-dimensional SE, which cannot be solved analytically.

The exciton states in QWs have been theoretically and numerically studied by many authors.[9,32–40] Miller *et al.*[32] have considered a two-dimensional exciton approximation for narrow QWs and obtained the exciton binding energy to be nearly four times that for the bulk crystal, R_x. Bastard *et al.*[9] and Greene *et al.*[33] employed the variational approach with various types of trial wave functions. In these works, the breakup of the $4R_x$ limit has been obtained for excitons in the QWs with finite barriers. Similar results have been obtained by Leavitt and Little[35] who applied the method based on the adiabatic approach. More recent paper of Gerlach *et al.*[38] describes a phenomenological model for the binding energy of an exciton in a QW. The authors compare the results of their model with the energies obtained by the variational approach with the prescribed trial function for the exciton wave function. The comparison shows a certain advantage in accuracy of the variational approach over the phenomenological model.

The variational approach became a standard one for the numerical study of the binding energy.[41–50] The trial wave functions used in the variational calculations of the exciton binding energy can be accurately chosen for two extreme cases. One of them is the wide QW; when the width, L, is much larger than the exciton Bohr radius, a_B, the motion of the exciton as a whole can be separated from the intrinsic motion of the electron and the hole. In this case, the trial function is a product of the hydrogen-like $1s$-function and a standing wave describing the quantization of the exciton motion in the wide QW.[16] Another case is the narrow QW, in which the quantum confined energy of the electron and the hole is much larger than their Coulomb coupling energy. Then, the separately obtained wave functions of the quantum confined electron and hole states are appropriate approximations.[38] The part of wave function taking into account the Coulomb interaction is usually modeled by a simple function with some parameters.[11,38] The precision of such approximations for the wide range of the QW widths between these two extreme cases has not been studied in detail so far.

The calculations of the radiative decay rate (or the oscillator strength) for the GaAs-based QWs have been carried out in several works.[51–56] In particular, the theoretical calculations by Iotti and Andreani[55] and D'Andrea *et al.*[56] predicted a general minimum of the oscillator strength at QW width $L \sim 2.5a_B$. This minimum defines the transition from the so-called weak exciton confinement ($L \gg a_B$) to the strong confinement ($L < a_B$), when the electron and the hole are separately localized. These studies have not been continued because of lack of the reliable experimental data due to low quality of the heterostructures. The experimental determination of the radiative characteristics has been done in a series of papers.[19,24,25,57–62] Recent studies of the radiative decay rate for high-quality QWs have been carried out by Poltavtsev *et al.*[24,25] In these papers, the general theoretical behavior has been experimentally confirmed. However, the spread of the experimental measurements and the shortage of the available theoretical calculations motivated us to fulfill this deficiency.

In the present paper, we provide the results of numerical solution of the SE for excitons in QWs with a degenerate valence band. Partial separation of the center-of-mass motion and cylindrical symmetry of the problem reduce the initial SE to the three-dimensional one. We have numerically solved the three-dimensional SE for the heavy-hole exciton in QWs of various widths and precisely calculated the exciton binding energy and the radiative decay rate.

The numerical solution of the problem has been done for the GaAs/AlGaAs and InGaAs/GaAs QWs, which are widely experimentally and theoretically studied now as the model heterostructures.[61,63] The obtained solutions are compared with results of the variational approach with the trial function proposed in Ref. 38. The results of the numerical experiments for different widths of the QWs are discussed in detail.

We also experimentally measured the reflectance spectra for several high-quality heterostructures with InGaAs/GaAs and GaAs/AlGaAs QWs grown by molecular beam epitaxy. An analysis of exciton resonances in the spectra using the theory described in Ref. 11 allowed us to obtain the radiative decay rates for excitons in these structures and to compare them with the numerically obtained results.

The paper is organized as follows. In Section II, we derive the three-dimensional SE from the complete exciton Hamiltonian. The direct and variational methods of numerical solution are described in Section III. Section IV presents results on the exciton binding energy and the wavefunction obtained by these two methods. Section V contains the obtained results for the radiative decay rate, their comparison with experimental data, as well as an analysis of the decay rate for the narrow and wide QWs. The approximations and comparison of the data obtained by two numerical methods are discussed in Section VI. Section VII summarizes main results of the paper. Additionally, some details of the numerical scheme and uncertainties are given in the Appendix.

II. MICROSCOPIC MODEL

The exciton in a QW is described by the SE with Hamiltonian

$$H = E_g + T_e + T_h - \frac{e^2}{\epsilon|\mathbf{r_e} - \mathbf{r_h}|} + V_e(\mathbf{r_e}) + V_h(\mathbf{r_h}). \quad (1)$$

Here, indices e and h denote the electron and the hole, respectively. We introduce the energy bandgap E_g, the kinetic operators for the electron, T_e, and for the hole, T_h, the relative electron-hole distance, $|\mathbf{r_e} - \mathbf{r_h}|$, the electron charge, e, and the dielectric constant, ϵ. The square QW potential $V_{e,h}(\mathbf{r_{e,h}}) = 0$ inside the QW, when $|z_{e,h}| < L/2$, and $V_{e,h}(\mathbf{r_{e,h}}) = V_{e,h}$ outside the QW, where $V_{e,h}$ are the conduction- and valence-band offsets.

In the effective-mass approximation,[30] the kinetic operator of the electron in the conduction band is explicitly given as $T_e = \mathbf{k}_e^2/(2m_e)$, where $\mathbf{k_e} = -i\hbar\nabla_e$ is the electron

momentum operator and m_e is the electron effective mass. The kinetic term of the hole in the valence band is given by the Luttinger Hamiltonian,[31] which can be written as

$$T_h = \frac{1}{m_0}\left[\left(\gamma_1 + \frac{5}{2}\gamma_2\right)\frac{\mathbf{k}_h^2}{2} - \gamma_2\left(k_{hx}^2 J_x^2 + k_{hy}^2 J_y^2 + k_{hz}^2 J_z^2\right) - 2\gamma_3\left(\sum_{m\neq n}\{k_{hm}, k_{hn}\}\{J_m, J_n\}\right)\right], \quad (2)$$

where γ_l with $l = 1, 2, 3$ are the Luttinger parameters, k_{hm}, $m = x, y, z$, are the components of the hole momentum operator, J_m are the 4×4 angular momentum matrices,[64] $\{J_m, J_n\} = (J_m J_n + J_n J_m)/2$ denotes the anticommutator, and m_0 is the mass of the free electron.

We consider only the diagonal part of the expression (2), assuming that the nondiagonal terms contribute little to the energy.[30] Therefore, we do not consider several effects extensively discussed in literature.[65,66] In particular, we ignore the heavy-hole–light-hole coupling, which is essential for the QWs of width $L > 150$ nm. For smaller widths, this effect is negligible. Further discussion on the reliability of the applied approximations is given in Section VI. Introducing the effective masses $m_{hxy} = m_0/(\gamma_1 \pm \gamma_2)$, $m_{hz} = m_0/(\gamma_1 \mp 2\gamma_2)$, of the heavy hole (upper sign) and light hole (lower sign), respectively, up to the constant energy gap E_g, we obtain the Hamiltonian

$$H_{\text{diag}} = \frac{\mathbf{k}_e^2}{2m_e} + \frac{\left(k_{hx}^2 + k_{hy}^2\right)}{2m_{hxy}} + \frac{k_{hz}^2}{2m_{hz}} - \frac{e^2}{\epsilon|\mathbf{r_e} - \mathbf{r_h}|} + V_e(\mathbf{r_e}) + V_h(\mathbf{r_h}). \quad (3)$$

In our study, we pay attention only to the heavy-hole excitons.

With the Hamiltonian (3), we come to the standard six-dimensional SE, $H_{\text{diag}}\Psi = E\Psi$, for the electron and the hole coupled by the Coulomb interaction.[67] The translational symmetry along the QW layer allows us to reduce this equation only to the four-dimensional one by separation of the center-of-mass motion in the (x, y)-plane. This motion is described by an analytical part of the complete wave function, Ψ. The relative motion of the electron and the hole in the exciton is described by the part $\psi(x, y, z_e, z_h)$ of the complete wavefunction, where $x = x_h - x_e$, $y = y_h - y_e$. One more dimension is eliminated by taking advantage of the cylindrical symmetry of the problem and introducing the polar coordinates (ρ, ϕ) for description of the relative motion. Representing the wave function in the form

$$\psi(x, y, z_e, z_h) = \psi(z_e, z_h, \rho)e^{ik_\phi\phi} = \frac{\chi(z_e, z_h, \rho)}{\rho}e^{ik_\phi\phi}, \quad (4)$$

where $k_\phi = 0, 1, 2, \ldots$, we proceed to the three-dimensional SE, which is numerically studied in the present paper. In Eq. (4), we introduce factor $1/\rho$ in order to fulfill the cusp condition[68] at $\rho = 0$.

Since the light interacts mainly with the ground $1s$ state of the exciton, we study the case when $k_\phi = 0$. In this case, the equation under consideration is written as[9]

$$\left(K - \frac{e^2}{\epsilon\sqrt{\rho^2 + (z_e - z_h)^2}} + V_e(z_e) + V_h(z_h)\right)\chi(z_e, z_h, \rho) = E_x\chi(z_e, z_h, \rho), \quad (5)$$

where the kinetic term reads

$$K = -\frac{\hbar^2}{2m_e}\frac{\partial^2}{\partial z_e^2} - \frac{\hbar^2}{2m_{hz}}\frac{\partial^2}{\partial z_h^2} - \frac{\hbar^2}{2\mu}\left(\frac{\partial^2}{\partial\rho^2} - \frac{1}{\rho}\frac{\partial}{\partial\rho} + \frac{1}{\rho^2}\right) \quad (6)$$

and $\mu = m_e m_{hxy}/(m_e + m_{hxy})$ is the reduced mass in the (x, y)-plane. The energy E_x denotes the exciton energy with respect to E_g.

In our study, Eq. (5) is solved numerically, and the energy and corresponding wave function are obtained for QWs of various widths and compositions of the QW layer and barriers. Other parts of the complete wave function are analytically known, though they are not of practical importance.

III. NUMERICAL METHODS

We performed the direct numerical solution of Eq. (5) for precise calculations of the exciton ground state energy E_x and the function $\chi(z_e, z_h, \rho)$. The exponential decrease in χ at large values of variables allows us to impose the zero boundary conditions for it at the boundary of some rectangular domain. The size of this domain varies from dozens of QW widths (for small widths) down to several QW widths (for large widths). Therefore, the studied boundary value problem (BVP) is formed by Eq. (5) and the zero boundary conditions at $\rho = 0$, some large value of ρ and at large positive and negative values of the variables $z_{e,h}$. Since Eq. (5) is the standard three-dimensional partial differential equation of elliptic type, the direct numerical solution of the BVP is feasible using available computational facilities. For this purpose, we employed the fourth-order finite-difference approximation of the derivatives on the equidistant grids of the equal step over three variables. It allowed us to solve Eq. (5) with the maximum theoretical uncertainty proportional to the square of the grid step because of a discontinuity of the potential. The precise values of the studied quantities are obtained by the extrapolation of the results of calculations as the grid step goes to zero. The details on the numerical scheme and theoretical uncertainties are described in the Appendix.

The nonzero solution of the homogeneous equation (5) with trivial boundary conditions can be obtained by the diagonalization of the matrix constructed from this equation. The obtained square matrix is large, nonsymmetric, and sparse. The typical size of the matrix is of the order of 10^6, so we keep in the calculations only nontrivial matrix elements of a few diagonals. The diagonalization of such a matrix is difficult; however, a small part of the spectrum can be easily obtained. Using the Arnoldi algorithm,[69] we have calculated the lowest eigenvalue of the matrix and the corresponding eigenvector. As a result, the ground state energy, E_x, and the corresponding wave function have been obtained for various widths of QW. The excited states can be obtained by this algorithm as the higher eigenvalues and eigenvectors.[70]

One of the alternative numerical methods is the approximate solution of the SE with Hamiltonian H defined by Eq. (1) using the variational approach. This technique has been applied by many authors.[9,11,33,38] In the framework of the variational approach, the ground state energy of the system with the Hamiltonian H is determined by the minimization of the functional

$$F = \frac{\langle\psi|H|\psi\rangle}{\langle\psi|\psi\rangle}, \tag{7}$$

with respect to some free parameters of the trial wave function ψ. For numerical calculation of the integrals in Eq. (7), one has to define the trial function. In Ref. 38, the trial wave function of the form

$$\psi(z_e, z_h, \rho) = \psi_e(z_e)\psi_h(z_h)\exp\left(-\frac{\alpha}{a_B}\sqrt{\rho^2 + \lambda(z_e - z_h)^2}\right) \tag{8}$$

is applied. Here, the functions $\psi_e(z_e)$ and $\psi_h(z_h)$ are the ground state wave functions of the free electron and the free hole, respectively, and α and λ are the varying parameters.

The shortcoming of the described variational approach is that the trial wave function has the prescribed form. Moreover, it assumes the partial separation of the variables, whereas the Coulomb potential in Eq. (5) does not allow that separation. Of course, one can define even more complicated trial functions,[33,71] but asymptotically (for small and large widths of QW), they have to be reduced to the function (8). This fact as well as the numerical simplicity of this ansatz provoked many authors to use it for calculation of the exciton binding energy, R_x. However, the accuracy of the results has not been studied in detail so far. The obtained wave function has also not been applied to calculate the exciton radiative characteristics.

We apply the described numerical algorithms for solving Eq. (5) with parameters for the GaAs/Al_xGa_{1-x}As and In_xGa_{1-x}As/GaAs QWs, which are widespread in the contemporary experimental studies. The parameters, presented in Table I, are general for such types of the QWs. In particular, they simulate the typical ratio of the band offsets at the GaAs/$Al_{0.3}Ga_{0.7}$As interface: $V_e/V_h \approx 2$. It is well known that the strain-induced effects are negligibly small in these structures due to nearly equal lattice constants of GaAs and AlAs. This fact is confirmed by the absence of the notable splitting of the heavy- and light-hole excitons in the GaAs/AlGaAs heterostructures with wide QWs.[63] For the InGaAs/GaAs QWs, the strain-induced effects strongly depend on the indium content due to considerable mismatch of the GaAs and InAs lattice constants. However, for planar structures, these effects do not disturb the rectangular profile of the QW potentials.[72] Therefore, they can be phenomenologically taken into account by changing the ratio V_e/V_h. We have chosen the ratio $V_e/V_h = 65/35$ for In concentration $x = 0.02$ and $V_e/V_h = 55/45$ for $x = 0.09$.[56] In the calculations, we have used the heavy-hole GaAs mass parameters reported in Ref. 38 as well as the In_xGa_{1-x}As ones from Ref. 73 For the latter ternary alloy, the linear interpolation on x of the mass parameters was used. For simplicity, we neglect the difference of the electron and hole masses in the QW and in the barrier layers. We ignore the discontinuity of the dielectric constant at the QW interfaces as well.[74] Reliability of these approximations is given in Section VI.

TABLE I. Material parameters used for solving the eigenvalue problem (5). The energy gap mismatch denoted as ΔE_g is calculated for AlGaAs heterostructure based on the data from Ref. 5, for InGaAs, it is based on Ref. 56. Bottom part of the table contains the effective masses for pure materials. These mass parameters for AlGaAs and InGaAs heterostructures are taken from Refs. 5 and 9, respectively. Masses for the InGaAs/GaAs are obtained by the linear interpolation on x.

Material parameters			
Heterostructure	GaAs/Al_xGa_{1-x}As	In_xGa_{1-x}As/GaAs	
x	0.3	0.02	0.09
ΔE_g (meV)	365.5	30	139
V_e/V_h	0.65/0.35	0.65/0.35	0.55/0.45
ϵ	12.53	12.53	
Mass parameters			
Material	GaAs	InAs	GaAs
m_e/m_0	0.067	0.026	0.067
m_{hz}/m_0	0.377	0.333	0.350
m_{hxy}/m_0	0.111	0.035	0.111
μ/m_0	0.042	0.015	0.042

IV. EXCITON BINDING ENERGY

The exciton binding energy, R_x, is defined by the exciton ground state energy, E_x, with respect to the quantum confinement energy of the electron, E_e, and the hole, E_h, in QW

$$R_x = E_e + E_h - E_x.$$

Energies E_e and E_h are obtained from solution of the corresponding one-dimensional SEs for the electron and the hole in QW.[10]

The calculations of the exciton binding energy have been carried out for various widths of the GaAs/$Al_{0.3}Ga_{0.7}$As QW. Fig. 1 shows the exciton binding energy, R_x, obtained

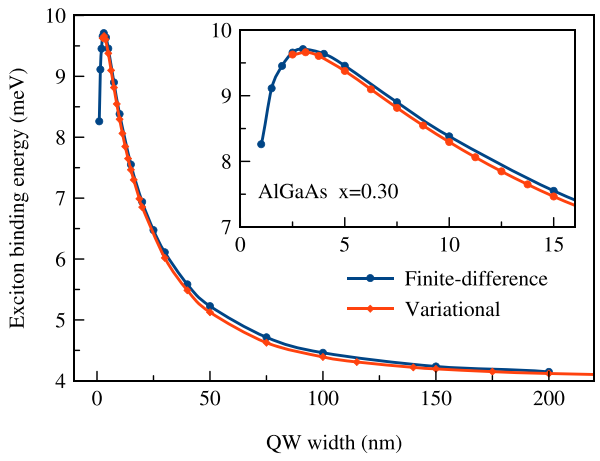

FIG. 1. Exciton binding energy, R_x, obtained by the finite-difference numerical solution of Eq. (5) (blue curve) and by the variational approach (red curve) for GaAs/$Al_{0.3}Ga_{0.7}$As QWs as a function of the QW width.

from the microscopic finite-difference calculations and the variational approach as a function of the QW thickness. The results of two methods coincide with the precision of 0.1 meV for QW widths $L \geq 2.5$ nm. This result means that the trial function (8) is a good approximation of the exciton wave function for the lowest state. The variational approach gives a bit smaller binding energy, which is the expectable result because the minimum of functional (7) is achieved for exact exciton wave function rather than for the trial function. This discrepancy seems to be unimportant for comparison with measurements due to typically larger uncertainties of experimental data. Therefore, both methods can be successfully applied for determination of the exciton binding energy.

The uncertainties of the finite-difference calculations of R_x come from the calculated values of E_x because the quantum confinement energies, E_e and E_h, can be calculated with an arbitrary high precision. We obtained the relative uncertainty of R_x to be smaller than 1% for $1.0 \leq L < 2.5$ nm and decreasing down to values smaller than 0.1% for wider QWs. The uncertainty is much smaller than the difference of the results obtained by two numerical methods.

The overall behavior of the binding energy within the microscopic model for QW widths $1 \leq L \leq 150$ nm can be approximated by the function: $R_x(L) = (3.5431L^2 + 146.694L)/(L^2 + 11.1758L + 6.0473)$ with the accuracy of 0.07 meV. The dependence of the parameters α and λ on L for the variational approach can be fitted by a phenomenological function

$$f(L) = f_0(\exp[-(L-L_0)/\Delta L_1] - \exp[-(L-L_0)/\Delta L_2]) + f_1,$$

where parameters for $\alpha(L)$ are $f_0 = -0.058$, $L_0 = 39$ nm, $\Delta L_1 = 50$ nm, $\Delta L_2 = 17$ nm, $f_1 = 1.064$, and for $\lambda(L)$ are $f_0 = -1.48$, $L_0 = -16$ nm, $\Delta L_1 = 56$ nm, $\Delta L_2 = 9$ nm, and $f_1 = 1.21$. The accuracy of these fits is of about 1.5%. In particular, for the QW of width $L = 200$ nm, where the exciton can be treated as the free one, $\alpha = 1.0604$, $\lambda = 1.1858$. These values are close to the expectable ones for the bulk crystal:[11] $\alpha_\infty = 1$, $\lambda_\infty = 1$.

Interestingly enough, the maximum binding energy is achieved at the QW width of about 3 nm. The binding energy decreases for thinner QWs due to the penetration of the carriers into the barriers. In the limit of very thick QWs, we obtained the values approaching the free exciton binding energy for the bulk crystal. From Fig. 1, one can see that, for our case, this energy is $R_x = 4.10 \pm 0.03$ meV, which slightly less than that reported in Ref. 30. It is worth noting that, for the QW width $L > 150$ nm, the obtained results may be less reliable due to omission of the nondiagonal Luttinger terms in our model.

Together with the exciton ground state energy, in the direct microscopic calculation, we have obtained the corresponding wave function. In the wide QWs, the wave function can be presented as a function $\varphi(Z, z, \rho) = \chi(z_e, z_h, \rho)/\rho$, depending of the relative coordinate, $z = z_e - z_h$, and center-of-mass coordinate, $Z = (m_e z_e + m_h z_h)/(m_e + m_h)$. The slices of $|\varphi(Z, z, \rho)|^2$ as functions of z and ρ for three different center-of-mass coordinates Z are shown in Fig. 2 for the QW width $L = 150$ nm. These slices show the probability distribution for the relative distance between the electron and the hole in the exciton. The center plot shows the exciton placed in the center of the QW while the side plots present the exciton near the QW interfaces. The magnitude of $|\varphi(Z, z, \rho)|^2$ for the side plots is in several orders smaller than for the center plot. It is normalized to the center plot for visibility. As seen from Fig. 2, the probability distribution is spherically symmetric at $Z = 0$ nm and reveals some distortion near the QW interfaces.

V. EXCITON-LIGHT COUPLING

A. Radiative decay rate

Exciton-light coupling is usually characterized by either the radiative decay rate or the oscillator strength.[11,16,52,53] The radiative decay rate, Γ_0, characterizes the decay of electromagnetic field emitted by an exciton ensemble after the pulsed excitation: $E(t) = E(0)\exp(iw_0 t - \Gamma_0 t)$. A consistent exciton-light coupling theory is presented, e.g., in the monograph of Ivchenko.[11] It provides the following expression for Γ_0:

$$\Gamma_0 = \frac{2\pi q}{\hbar\epsilon}\left(\frac{e|p_{cv}|}{m_0\omega_0}\right)^2 \left|\int_{-\infty}^{\infty} \Phi(z)\exp(iqz)dz\right|^2, \qquad (9)$$

where $q = \sqrt{\epsilon}\omega/c$ is the light wave vector, ω_0 is the exciton frequency, $|p_{cv}|$ is the matrix element of the momentum operator between the single-electron conduction- and valence-band states, and $\Phi(z) \equiv \psi(z_e = z, z_h = z, \rho = 0)$.

The simplification of Eq. (9) used in Refs. 53 and 55 takes into account that the QW width is much smaller than the light-wave length $2\pi/q$. It allows one to replace $\exp(iqz)$ in the integral by unity. In this case, the radiative decay rate Γ_0 is closely related to the oscillator strength per unit area,[53]

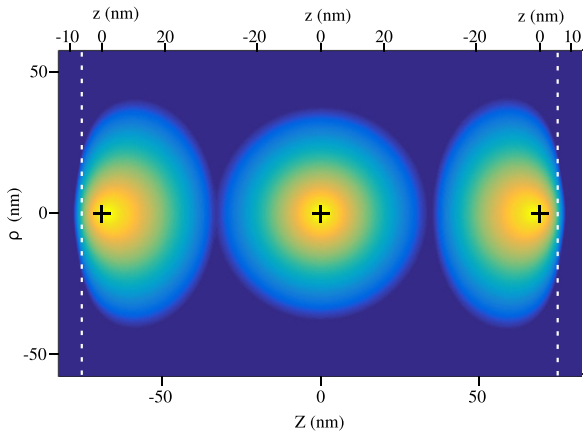

FIG. 2. The slices of the exciton wave function squared, $|\varphi(Z, z, \rho)|^2$, as functions of relative coordinates (z, ρ) for three different center-of-mass coordinates $Z = -69, 0, 69$ nm of the exciton. The QW width, L, equals to 150 nm. The coordinates of the center-of-masses of the excitons are depicted by small crosses. The QW interfaces are drawn by the dashed vertical lines. The probability for the electron and the hole to be at distance $r = \sqrt{z^2 + \rho^2}$ is shown in the logarithmic scale. The magnitude of the side plots is normalized to the central one.

f/S, by the formula $\Gamma_0 = (\pi e^2 f)/(n m_0 c S)$, where n is the refractive index ($\sqrt{\epsilon} = n + ik$).

The wave function obtained from the microscopic calculation allowed us to calculate the radiative decay rate Γ_0 of the exciton ground state according to Eq. (9). We calculated Γ_0 for GaAs/$Al_{0.3}Ga_{0.7}As$ QWs of various widths from 1 nm to 300 nm. In the calculations, $|p_{cv}|^2 = m_0 E_p/2$, where $E_p = 28.8$ eV for GaAs and $E_p = 21.5$ eV for InAs are taken from Ref. 73. The exciton frequency ω_0 is calculated using bandgap $E_g = 1.520$ eV for GaAs[11] and parameters listed in Table I.

Fig. 3 shows the radiative decay rate in energy units, $\hbar\Gamma_0$, as a function of the QW width. The radiative decay rate reaches its maximum at the QW width of about 130 nm, which approximately corresponds to a half of the light wavelength in the QW material, $\lambda(\text{GaAs}) = \lambda(\text{vac})/n(\text{GaAs}) = 230$ nm, where $n(\text{GaAs}) = 3.6$ is the refractive index of GaAs at the photon energy $\hbar\omega = E_g$. So, this maximum of Γ_0 corresponds to the maximal overlap of the exciton wave function $\Phi(z)$ and the light wave (see Eq. (9)).

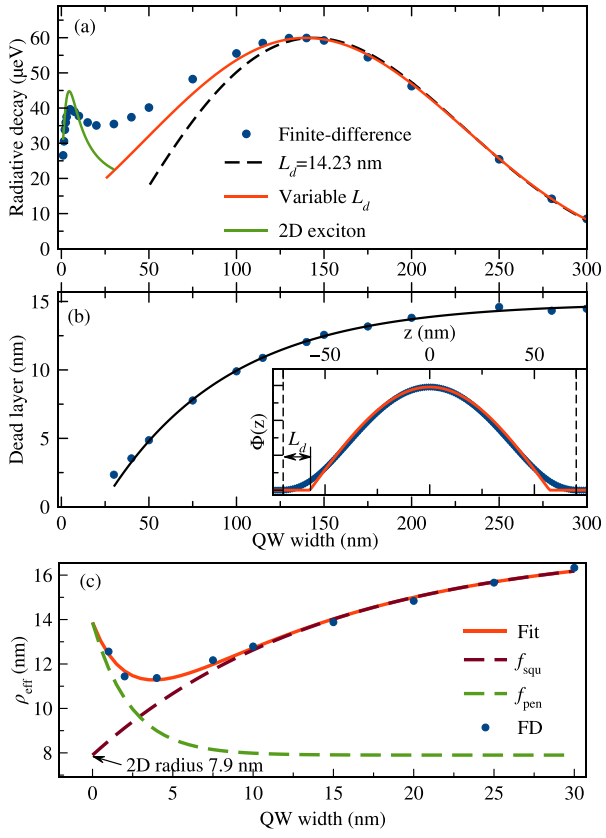

FIG. 3. (a) The radiative decay rate in energy units, $\hbar\Gamma_0$, versus QW width, L. Blue dots are obtained in the finite-difference calculation. The dashed line corresponds to Γ_0 for the bulk exciton in a QW with infinite barriers and constant dead layer $L_d = 14.23$ nm. The solid red line is the calculation with the variable dead layer shown in (b). The green solid line corresponds to Γ_0 in the 2D exciton model with the varying effective radius ρ_{eff} shown in (c). (b) The variable dead layer as a function of QW width. The inset: function $\Phi(z)$ and its approximation by $\cos(\pi Z/L^*)$ for QW with $L = 150$ nm. The two-side arrow marked "L_d" illustrates definition of the dead layer. (c) Effective 2D exciton radius, ρ_{eff}, extracted from the finite-difference (FD) calculations (solid points) for the QW widths 0–30 nm and its approximation by the function (13) (solid curve) with parameters: $C_1 = 9.5 \pm 0.4$ nm, $L_1 = 14 \pm 1$ nm, $C_2 = 6.0 \pm 0.5$ nm, $L_2 = 2.4 \pm 0.3$ nm. Dashed curves show contributions $f_{\text{squ}}(L)$ and $f_{\text{pen}}(L)$ in Eq. (13).

As the QW width decreases, Γ_0 also decreases due to the diminishing of the overlap integral in Eq. (9). For small QW widths, however, Γ_0 grows, which correlates with the increase in the exciton binding energy (compare with Fig. 1). Therefore, we may suppose that this maximum of Γ_0 is caused by squeezing of the exciton in the narrow QWs by the QW potential. The squeezing gives rise to the increase in the probability to find electron and the hole in the same position ($z_e = z_h$ and $\rho = 0$). Between these maxima of Γ_0, there is a minimum for the QW width of about 30 nm, which corresponds to the exciton Bohr diameter. The presence of such minimum was earlier pointed out by Iotti and Andreani.[55]

We compared our results with two simple approximations: the exciton in the bulk semiconductor for wide QWs and two-dimensional approximation for narrow QWs. Both the approximations are shown in Fig. 3 by various curves. The wave function of the exciton in the bulk semiconductor is given as[11]

$$\psi(Z, r) = \sqrt{\frac{2}{\pi a_B^3 L^*}} \cos\left(\frac{\pi}{L^*} Z\right) \exp\left(-\frac{r}{a_B}\right), \qquad (10)$$

where r is the electron-hole distance, $L^* = L - 2L_d$ is the effective QW width obtained from the QW width L, and the dead layer L_d.[75–77] The part of the wave function (10) depending on Z is represented only by function $\cos(\pi Z/L^*)$. It leads us to the conventional definition of the dead layer, which is the distance from the QW interface to the point where the cosine approximation of the exciton wave function becomes zero. This definition of the dead layer is illustrated by the inset of Fig. 3(b). Substituting the wave function (10) in Eq. (9), one can calculate the radiative decay rate in a QW with infinite barriers and a constant dead layer $L_d = 14.23$ nm. It is shown by dashed curve in Fig. 3(a). One can see that this approximation is acceptable for the QW widths $L \geq 140$ nm.

A better approximation of the dependence $\Gamma_0(L)$ can be achieved using the variable dead layer.[71] We extracted the variable dead layer by fitting the function (10) at $r = 0$ to the numerically obtained $\Phi(z)$ [see inset of Fig. 3(b)]. The extracted values of L_d are shown in Fig. 3(b) by solid points. The dependence of L_d on the QW width L can be well approximated by the phenomenological formula: $L_d = a(1 - \exp(-L/L_0)) + b$, where $a = 20.6 \pm 0.5$ nm, $L_0 = 70 \pm 2$ nm, and $b = -5.7 \pm 0.7$ nm. Using this approach and $a_B = 14.23$ nm, we obtained more accurate approximation of $\hbar\Gamma_0(L)$, which is shown in Fig. 3(a) by a red solid curve. This approximation is appropriate for the QW widths down to 100 nm.

For narrower QWs, both the bulk exciton wave function and the idea of variable dead layer are no longer applicable. Instead, for thin QWs, we implemented the two-dimensional (2D) exciton approximation. The wave function of the 2D exciton has the form[11]

$$\psi(z_e, z_h, \rho) = \psi_e(z_e)\psi_h(z_h) \sqrt{\frac{2}{\pi \rho_{\text{eff}}^2}} \exp\left(-\frac{\rho}{\rho_{\text{eff}}}\right), \qquad (11)$$

where ρ_{eff} is the effective 2D exciton radius, $\psi_e(z_e)$ and $\psi_h(z_h)$ are wave functions of the free electron and free hole in a QW with finite barriers. Function (11) is the solution of eigenvalue problem with the Hamiltonian (1) and 2D Coulomb potential, $-e^2/(\epsilon\rho)$. In the true 2D exciton problem, ρ_{eff} is the 2D Bohr radius

$$\rho_{2D} = \frac{\hbar^2\epsilon}{2\mu e^2}, \tag{12}$$

which is twice smaller than a_B.

The exciton in the QWs with finite heights of the barriers does not reach two-dimensional limit due to penetration of the exciton wave function into the barriers. Therefore, we consider ρ_{eff} as a characteristic parameter. We fitted the wave function (11) to the numerically obtained wave function $\Phi(z)$ by varying ρ_{eff}. The extracted effective 2D exciton radius values are presented in Fig. 3(c). It is seen that ρ_{eff} decreases as $L \to 4$ nm and then increases again as $L \to 0$. This behavior is well described by a phenomenological function

$$\begin{aligned} f(L) &= f_{\text{squ}}(L) + f_{\text{pen}}(L) \\ &= [\rho_{2D} + C_1(1 - e^{-L/L_1})] + [C_2 e^{-L/L_2}]. \end{aligned} \tag{13}$$

The first part of this function, $f_{\text{squ}}(L)$, decreases with $L \to 0$ down to the 2D-limit given by Eq. (12), $\rho_{2D} = 7.9$ nm for GaAs, and reflects the squeezing of exciton in narrow QWs. Another one, $f_{\text{pen}}(L)$, increases as $L \to 0$ and reflects the penetration of exciton into the barrier. Using this dependency, we calculated $\hbar\Gamma_0$ for the 2D exciton model (see Fig. 3(a)). As it is seen, this model, even with varying ρ_{eff}, is adequate in terms of the radiative decay rate only for narrow QWs $L \leq 15$ nm.

The described approximations are applicable for narrow or wide QWs separately. The excitons in QWs of intermediate widths are not described by these models. Only the direct microscopic calculation provides the precise values of the radiative decay rate for the wide range of QW widths.

B. Experimental determination of Γ_0

Exciton reflectance spectra can be used to obtain radiative decay rate. According to the theory summarized in Ref. 11, the amplitude reflectance coefficient of a QW with an exciton resonance is given as

$$r_{QW} = \frac{i\Gamma_0}{\tilde{\omega}_0 - \omega - i(\Gamma + \Gamma_0)}, \tag{14}$$

where $\tilde{\omega}_0$ is the renormalized exciton resonance frequency and ω is the frequency of the incident light. The nonradiative decay rate Γ in Eq. (14) takes into account resonance broadening due to nonradiative processes. Reflectance r_{QW} is strictly related to the reflectance coefficient of the whole heterostructure, R, which, in turn, can be measured in experiment.

For a single QW heterostructure, the relationship between R and r_{QW} can be found in Ref. 11. In a structure with several QWs as those used in our study, the reflectance coefficient is generalized to

$$R = \left| \frac{r + \sum_j r_{\text{QW}j} e^{i\phi_j}}{1 + r\sum_j r_{\text{QW}j} e^{i\phi_j}} \right|^2. \tag{15}$$

Here, r is the Fresnel reflectance coefficient from the surface of a heterostructure and ϕ is the phase shift of the light wave reflected by the QW with respect to that reflected by the structure surface. The index j numerates the resonances observed experimentally. Effectively, Eqs. (14) and (15) are the direct relations between the reflectance R and the radiative decay rate Γ_0.

For comparison of the theoretical modeling with experimental results, the high-quality heterostructures with QWs grown by molecular beam epitaxy have been selected for study of their reflectance spectra. These heterostructures contain several QWs separated by relatively thick barrier layers, which uncouple the wells. The spectra were measured using a simple setup consisting of a white light source, a cryostat, and a spectrometer equipped with a CCD camera. Special precautions have been taken to accurately calibrate the absolute value of reflectance. For this purpose, a monochromatic light of a continuous-wave titanium-sapphire laser was used to measure the reflectance at a spectral point beyond the exciton resonances.

Fig. 4 demonstrates examples of the reflectance spectra (blue curves) for the GaAs/$Al_{0.3}Ga_{0.7}As$ and $In_{0.02}Ga_{0.98}As$/GaAs heterostructures measured at 4 K. We used Eq. (15) to fit the spectra with Γ_0, Γ, ω_0, and ϕ as the fitting parameters for each resonance (red curves). The radiative decay rate in energy units, that is, the radiative broadening, $\hbar\Gamma_0$, as well as

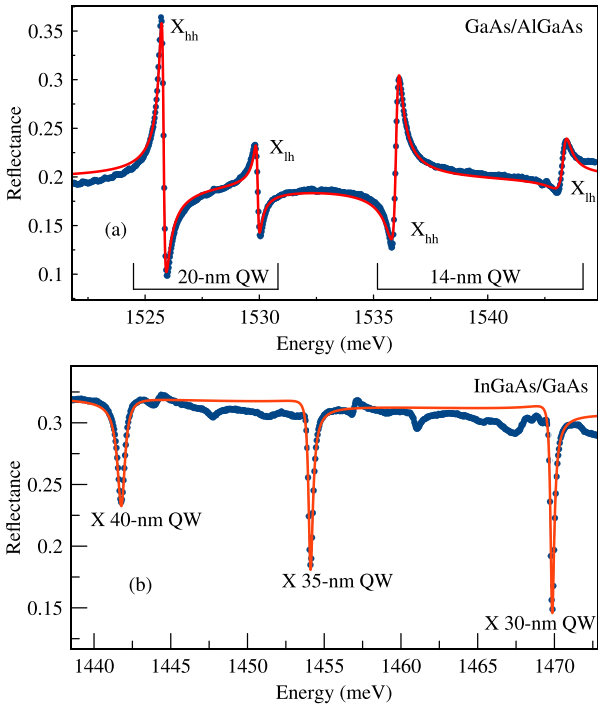

FIG. 4. (a) The experimental reflectance spectrum (blue curve) of the heterostructure with two GaAs/$Al_{0.3}Ga_{0.7}As$ QWs as well as the fit (red curve) of the spectrum. The ground heavy- and light-hole exciton states are denoted by X_{hh} and X_{lh}, respectively. (b) The same is for the heterostructure with three $In_{0.02}Ga_{0.98}As$/GaAs QWs. Ground heavy-hole exciton states are denoted by X.

TABLE II. The radiative, $\hbar\Gamma_0$, and nonradiative, $\hbar\Gamma$, decay rates in energy units (μeV). The data were extracted from the measured spectra of heterostructures with QWs of various widths, L (nm). The standard deviations obtained in the fitting are also given.

Heterostructure	L	x	$\hbar\Gamma_0(X_{hh})$	$\hbar\Gamma_0(X_{lh})$	$\hbar\Gamma(X_{hh})$	$\hbar\Gamma(X_{lh})$
GaAs/Al$_x$Ga$_{1-x}$As	14	0.30	37	15	123	197
	20	0.30	35	11	67	74
In$_x$Ga$_{1-x}$As/GaAs	2	0.02	30		93	
	3	0.03	27		42	
	3	0.02	26		65	
	30	0.04	38		130	
	35	0.05	35		157	
	40	0.07	37		285	
	95	0.02	58		117	
Standard deviation			2%	5%	3%	6%

the nonradiative one, are presented in Table II for a series of QW heterostructures. The nonradiative broadening originates from the thermal and static disorder, e.g., on the interfaces. The first one is suppressed by cooling the sample, whereas the second one is small due to a high quality of the grown structures. We fitted only the ground heavy-hole and light-hole exciton states. In the InGaAs spectra, we were able to reliably determine only the heavy-hole exciton resonances because the light-hole ones are significantly detached by the strain.[72]

The shape of exciton resonances (peaks, dispersion-like curves, or dips) is known to be defined by the phase ϕ_j in Eq. (15) related to the QW-to-surface distance for the given sample. In Fig. 4(a), for example, the resonant profiles for the 20-nm QW and for the 14-nm QW are different due to different QW-to-surface distances in this heterostructure. Otherwise, the shapes of the exciton resonances in the three InGaAs QWs are similar [see Fig. 4(b)]. In this case, QWs are shifted by a distance of about λ(GaAs) with respect to each other and, therefore, their phases are approximately equal. In case of the peak-shaped exciton resonance, $\hbar(\Gamma+\Gamma_0)$ corresponds to the half-width at half-maximum (HWHM) of the peak. Relatively small peculiarities of the spectrum observed in Fig. 4(b) are the excited quantum confined exciton states, which are beyond the scope of the present paper.

Experimentally obtained radiative decay rates for heavy-hole excitons are compared to the calculated data in Fig. 5. In the calculations, we simulated GaAs/Al$_{0.3}$Ga$_{0.7}$As and In$_{0.02}$Ga$_{0.98}$As/GaAs heterostructures with 365.5 meV and 30 meV band offsets (see Table I), respectively. The calculations indicate that the radiative decay rate for GaAs/AlGaAs heterostructure grows as L diminishes in the range $L=5-20$ nm. The experimentally obtained values of $\hbar\Gamma_0$ for the studied GaAs/AlGaAs structures exhibit a good agreement with the calculated results. In particular, they support the tendency of increase in $\hbar\Gamma_0$ with decrease in the QW width in this range. This tendency is also confirmed by many experimental data in Ref. 24.

Experimental results for InGaAs/GaAs heterostructures demonstrate a trend of $\hbar\Gamma_0$ to diminish with decrease in the QW width down to $L\approx 5$ nm, which is in agreement with

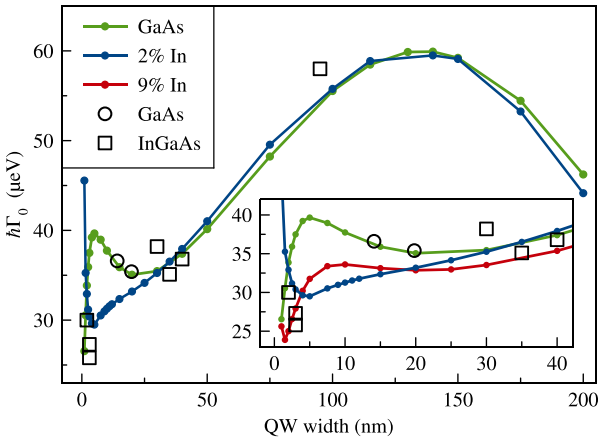

FIG. 5. The calculated radiative decay rate for In$_x$Ga$_{1-x}$As/GaAs QWs with 2% and 9% of In (blue and red curves, respectively) as well as for GaAs/Al$_{0.3}$Ga$_{0.7}$As QWs (green curve). The empty squares and circles show the experimental data for InGaAs/GaAs and GaAs/AlGaAs QWs, respectively.

the calculations. At the same time, the experimental data are more spread around the values expected from the computation. A large spread of the data is also observed in Ref. 25. We explain this spread mainly by the indium concentration variation from one sample to another in the range of $2\%-7\%$. We should note that high mobility of indium atoms during the growth process makes InGaAs heterostructures less predictable as compared to AlGaAs ones, in particular, due to the segregation effect.[78]

C. $\hbar\Gamma_0$ in shallow quantum wells

The large difference in behavior of the radiative decay rate for GaAs/AlGaAs and InGaAs/GaAs in the range of small QW widths requires a particular analysis. We believe that this difference is related to different depths of the QWs. To check this assumption, we carried out computations of $\hbar\Gamma_0$ for different concentrations x in the In$_x$Ga$_{1-x}$As/GaAs heterostructures that results in different heights of the QW barriers. In particular, for $x=0.02$ and 0.09, the barriers are $V_e=19.5$ meV and $V_e=76.5$ meV, respectively.

In the inset of Fig. 5, the radiative decay rates for different heterostructures are shown. It demonstrates the evolution of the radiative decay rate in narrow QWs with the growth of the barrier height. As the height increases with growing of x, the peak of $\hbar\Gamma_0$ becomes more pronounced and its maximum is shifted to the lower QW widths. As we noted above, the peak at $L\approx 5$ nm for the GaAs/AlGaAs QWs is formed due to exciton squeezing by the QW potential.

In the case of In$_x$Ga$_{1-x}$As/GaAs QWs with small concentration of indium, $x=0.02$, there is no peak of $\hbar\Gamma_0$ at the small QW widths. This is an indication of the weak exciton squeezing due to the small QW potential depth. For the In$_x$Ga$_{1-x}$As/GaAs QWs with $x=0.09$, some intermediate behavior is observed due to the intermediate height of the barriers.

To understand this behavior, we applied the 2D exciton model described in Sec. V A and extracted $\rho_{\rm eff}$ for In$_x$Ga$_{1-x}$As/GaAs QWs with 2% and 9% of indium [see Fig. 6(b)]. The dependence $\rho_{\rm eff}(L)$ for the shallow QW ($x=0.02$)

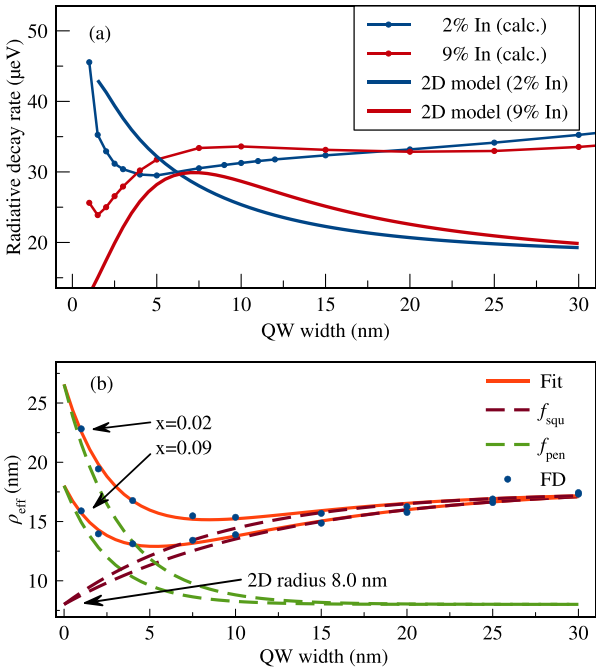

FIG. 6. (a) The calculated radiative decay rate for the $In_xGa_{1-x}As/GaAs$ QWs with 2% and 9% of indium (curves with points) in comparison with the 2D exciton model (smooth curves). Blue curves represent 2% of indium in the heterostructures, while 9% of indium is shown in carmine. (b) The fitted effective 2D exciton radius ρ_{eff} (solid points) for 2% and 9% of indium as well as the phenomenological approximations (see the text).

reveals the weak minimum, which is an indication of the weak squeezing of the exciton. Correspondingly, no maximum of $\hbar\Gamma_0$ should be observed for these QWs. Indeed, the calculated width dependence of $\hbar\Gamma_0$ shows monotonic rise with $L \to 0$ (see Fig. 6(a)). Curve $\rho_{eff}(L)$ for deeper QW ($x = 0.09$) shows the noticeable minimum at $L \approx 5$ nm that points out to an exciton squeezing. As a result, a maximum of $\hbar\Gamma_0$ appears [Fig. 6(a)].

The rapid growth of $\hbar\Gamma_0$ at $L \to 0$ in the InGaAs/GaAs QWs with 2% of indium is observed (see Fig. 6(a)). An analysis has shown that this growth is explained by the stronger penetration of exciton into the barriers as compared to the deeper InGaAs QWs with 9% of indium. Due to the penetration, the overlap of the exciton wave function $\Phi(z)$ and the light wave increases [see Eq. (9)] and, correspondingly, the radiative decay rate increases as $L \to 0$.

VI. DISCUSSION

The numerical results presented above have been obtained with a good accuracy. For the exciton binding energy, it is much less than 1% and for the radiative decay rate, it is better than 4% (for $L < 50$ nm). At the same time, these results are obtained in the framework of some simplifications of exciton problem, which should be discussed in detail.

First of all, we should note that for the QW widths $L < 2.5$ nm, the EFA may be rough. Therefore, other approaches like tight-binding model, all-band pseudopotential method, or account for the interface short-range corrections can be used to obtain reliable results for this range of QW widths.[79–81]

In our model, we disregard the mismatch of effective masses of carriers and of dielectric constants in the QW material and in the barrier layers. The mass mismatch leads to an increase in the binding energy by about 10% for narrow GaAs/AlGaAs QWs of width $L < 5$ nm, when the exciton wave function significantly penetrates into the barriers.[43] The discontinuity of the dielectric constant further increases the binding energy by about 5%.[51] For larger L, the effect of the mass mismatch disappears, and only the discontinuity of the dielectric constants contributes to the binding energy shift $\Delta R_x < 0.5$ meV.[55,56] The radiative decay rate is noticeably affected by the mass mismatch for the narrow GaAs/AlGaAs QWs with $L < 5$ nm only. We estimate that, for such widths, $\hbar\Gamma_0$ increases by about 15%. For larger widths, the effect of the mass mismatch rapidly decreases and almost vanishes for $L = 10$ nm. The change of $\hbar\Gamma_0$ due to the mismatch of dielectric constants seems to be negligible. For the InGaAs/GaAs, the effect of both mismatches on the R_x and $\hbar\Gamma_0$ is unobservable for any QW widths due to the small indium concentration.

Our model has some limitations for wide QWs. In particular, we ignored the coupling of the heavy- and light-hole band, which is described by the off-diagonal terms in the Luttinger Hamiltonian (2). For the unstrained GaAs/AlGaAs heterostructures, this coupling becomes essential for the QWs of width $L > 150$ nm, where the energy distance between the heavy- and light-hole exciton states is comparable with the contribution from the off-diagonal terms. However, the effect of this coupling is relatively small. Our estimates show that the mixing effect for the 80 nm GaAs/AlGaAs QW gives rise to the exciton energy shift of about 10 μeV. The exciton binding energy obtained in our work for the 200-nm GaAs/AlGaAs QW differs only by 5% from the bulk value reported in Ref. 30, where the heavy-hole–light-hole coupling was taken into account. The radiative decay rate is also changed by the same order of magnitude. This difference is not important for the analysis of experimental data because of unavoidable experimental uncertainties. For the InGaAs/GaAs heterostructures, the strain-induced heavy-hole–light-hole band splitting strongly suppresses the coupling, and the off-diagonal terms do not play any role.

In the wide unstrained QWs, the energy distance between the adjacent exciton quantum confined states may be smaller than the radiative broadening, so they cannot be considered as separated exciton resonances. In this case, the exciton-light coupling should be considered for several resonances simultaneously.[82] Besides, the dielectric constant should be replaced to a dielectric function depending on the wave vector of the exciton propagating across the QW.[11] Both these effects are considered in the model of excitonic polaritons extensively discussed in literature for thin crystals and wide QWs.[63,76,83]

The limitations described above show that our model provides reliable results for the GaAs/AlGaAs QWs of widths $L = 5 - 150$ nm and for the InGaAs/GaAs QW of widths $L = 2.5 - 200$ nm. We should stress that the model is applicable for the broad range of the QW widths between the

very narrow and very wide QWs, where the approximate methods are unreliable. In the range $L < 30$ nm, the calculated radiative decay rate has been compared with the data obtained by D'Andrea *et al.*[56] for InGaAs/GaAs QWs. The observed small difference, less than 3 μeV, supports the correctness of the results obtained in our work as well.

In Section IV, we have shown that the exciton binding energy is obtained quite precisely by the finite-difference method as well as by the variational approach with prescribed trial function (8). The good agreement of the results of two methods indicates that the chosen trial function is appropriate for the wide range of QW thicknesses. It seems that, for each QW width, the varying parameters allow one to properly scale the trial function and, thus, to simulate the exact ground state wave function. Therefore, besides the binding energies, the wave functions obtained by two methods should also be similar. In this context, it is interesting to compare the radiative decay rates obtained using these two methods. The wave function of the exciton ground state obtained by the variational approach for the GaAs/$Al_{0.3}Ga_{0.7}As$ heterostructure has been used to calculate Γ_0. The results obtained by two methods are compared in Fig. 7. As seen, the relative difference of the calculated values (of about 10%) is larger than that for the exciton binding energies. In particular, for $L \sim 5$ nm, the variational approach gives greater radiative decay rate than the direct numerical solution. Nevertheless, such difference is generally not so important for comparison with experimental data because their spread (see Fig. 5 and Refs. 24 and 25) exceeds this discrepancy. Therefore, we may conclude that the variational approach with the proposed in Ref. 38 anzatz (8) is appropriate for calculation of the exciton binding energy as well as the radiative decay rate.

The exciton binding energy and radiative decay rate are the integral characteristics of the exciton states. Although the comparison showed us that these characteristics are similar, the wave functions obtained by different methods may differ in some details. This difference may affect other properties of excitons, e.g., sensitivity to a magnetic field.[13] So, for the

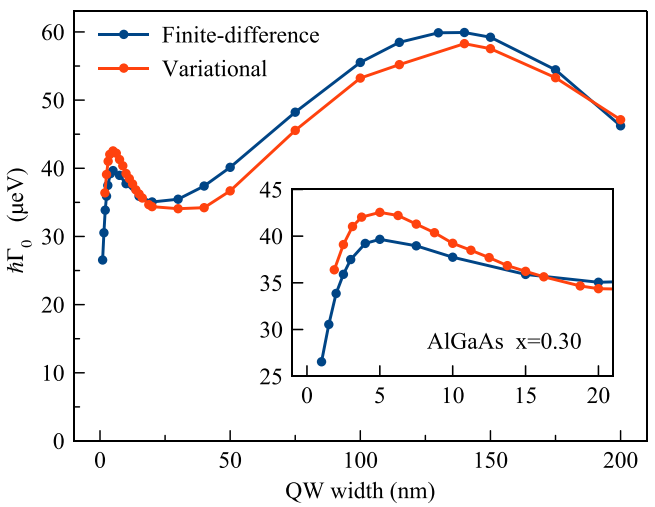

FIG. 7. The radiative decay rate in energy units obtained for GaAs/AlGaAs QWs by the microscopic finite-difference calculation in comparison to the results from the variational approach as a function of the QW width.

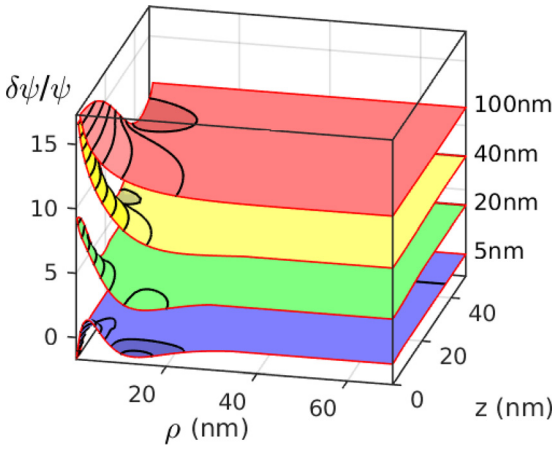

FIG. 8. The relative difference (in percent) of the wave functions of excitons in GaAs/AlGaAs QWs obtained by the precise microscopic calculation and by the variational approach as a function of two variables: ρ, $z = z_e = z_h$ for QW widths $L = 5, 20, 40, 100$ nm (from bottom to top). The functions are shifted vertically for visibility.

future prospects, we have compared the wave functions themselves. Fig. 8 shows the difference (in percent) of the exciton wave functions obtained by two methods as a function of ρ and z for several widths of the GaAs/AlGaAs QWs. The main difference of the wave functions is observed near the $z = 0$, $\rho = 0$ point. This difference for small L does not exceed 5% and rapidly decreases with the z and ρ rise. For larger L, the difference is larger but also rapidly decreases as z and ρ grow.

VII. CONCLUSIONS

In the present paper, we have numerically solved the three-dimensional SE and obtained the exciton binding energy as well as the ground state wave function. The studied SE was deduced from the electron-hole Hamiltonian with the Luttinger term for the valence band taking into account only the heavy-hole excitons. The SE was solved by two methods: the direct one and the variational one. The variational method has been used by number of author who studied this problem. The direct microscopic solution using the fourth-order finite-difference scheme has been carried out for the first time. It allowed us to precisely calculate the ground state and the exciton radiative decay rate.

We obtained the radiative decay rates for GaAs/AlGaAs and InGaAs/GaAs heterostructures for various QW widths $1 \leq L \leq 200$ nm and compound concentrations. We found that, since the different concentrations lead to the different magnitudes of band offsets, the behavior of the radiative decay rate for narrow QW widths ($2 < L \leq 10$ nm) strongly depends on the concentration. The increase in the concentration leads to the higher barriers and to growth of the peak of the radiative decay. For very narrow QWs ($L \leq 2$ nm), the radiative decay rate also behaves differently. If the QW is shallow, then the radiative decay rate grows as $L \to 0$. Instead, if the QW is deep, then it seems to be decreasing.

The obtained wave functions were used to test some simple models, namely, the 3D exciton model (exciton in the bulk semiconductor) and the 2D exciton model. We have

shown that these models are applicable only for wide and narrow QWs, respectively. The parameters of the models and the limits of applicability were estimated.

The comparison of the exciton binding energies obtained by the direct microscopic calculation and by the variational approach showed a very good agreement with the discrepancy of less than 0.1 meV for a wide range of QW widths. The analogous comparison of the radiative decay rates gave the similar overall behavior of these quantities, but larger differences (up to 10%). Nevertheless, even for narrow QWs, this difference can be considered as unimportant because the available experimental data are more spread for these QWs. As a result, both numerical methods can be successfully used for the calculation of the exciton binding energy and the radiative decay rate. The experimental measurements of the radiative decay rate for several QW widths presented in the paper are consistent with the results of the calculations.

ACKNOWLEDGMENTS

The authors would like to thank Alexander Levantovsky for providing the advanced plotting and curve fitting program MagicPlot Pro. Financial support from the Russian Ministry of Science and Education (Contract No. 11.G34.31.0067), SPbU (grants No. 11.38.213.2014 and No. 11.38.241.2015), RFBR (grants No. 14-02-00326 and No. 16-02-00245) and DFG in the frame of Project ICRC TRR 160 is acknowledged. The authors also thank the SPbU Resource Center "Nanophotonics" (www.photon.spbu.ru) for the samples studied in present work. Some calculations were carried out using the facilities of the "Computational Center of SPbU."

APPENDIX: NUMERICAL DETAILS

In our study, we employ the well known finite-difference (FD) approximation[84–86] of the derivatives in Eq. (5) due to its robustness as well as sparse and relatively simple form of the obtained matrix equation. We consider the BVP for Eq. (5) at the domain $[-Z_e/2, Z_e/2] \times [-Z_h/2, Z_h/2] \times [0, R]$ over variables z_e, z_h, and ρ, respectively, and specify the homogeneous boundary conditions at the boundaries. The equidistant grids over each variable are introduced by the formulas $z_{e,k} = k\Delta_{z_e} - Z_e/2$, $z_{h,l} = l\Delta_{z_h} - Z_h/2$, $\rho_m = m\Delta_\rho$, where $\Delta_{z_{e,h}} = Z_{e,h}/(N_{z_{e,h}} + 1)$, $\Delta_\rho = R/(N_\rho + 1)$ are the grid steps and the indices k, l, and m go from 1 to some integer values N_{z_e}, N_{z_h}, and N_ρ, respectively. We use the central fourth-order FD formula for approximation of the second partial derivative of $\chi(z_e, z_h, \rho)$ with respect to z_e

$$\frac{-\chi_{k-2,l,m} + 16\chi_{k-1,l,m} - 30\chi_{k,l,m} + 16\chi_{k+1,l,m} - \chi_{k+2,l,m}}{12\Delta_{z_e}^2}. \tag{A1}$$

Here, the unknown wave function on the grid $\chi(z_{e,k}, z_{h,l}, \rho_m)$ is denoted as $\chi_{k,l,m}$. The same FD formula is employed for the second derivative with respect to z_h. The wave function χ at the knots beyond the considered domain over z_e and z_h is taken to be negligible due to its exponential decrease in this region. We apply the noncentral fourth-order FD formulas for approximation of the first and second partial derivatives of $\chi(z_e, z_h, \rho)$ with respect to ρ

$$\frac{-3\chi_{k,l,m} - 10\chi_{k,l,m+1} + 18\chi_{k,l,m+2} - 6\chi_{k,l,m+3} + \chi_{k,l,m+4}}{12\Delta_\rho}, \quad \frac{10\chi_{k,l,m} - 15\chi_{k,l,m+1} - 4\chi_{k,l,m+2} + 14\chi_{k,l,m+3} - 6\chi_{k,l,m+4} + \chi_{k,l,m+5}}{12\Delta_\rho^2}. \tag{A2}$$

It allows us to satisfy the trivial boundary condition at $\rho = 0$ and to avoid knots $\rho_m < 0$. At the knots $\rho_m > R$, the wavefunction is also assumed to be zero. It should be noted that this assumption is possible only if the considered domain is large enough.

In the calculations, the grid steps over each variable have been taken to be the same, $\Delta = \Delta_{z_e} = \Delta_{z_h} = \Delta_\rho$, and multiply associated with the QW width. The formulas (A1) and (A2) define the theoretical uncertainty of the numerical solution of order of Δ^4 as $\Delta \to 0$. However, the discontinuity of the square potential at the QW interfaces decreases the convergence rate of the solution over z_e and z_h to order of Δ^2, whereas the convergence rate over variable ρ is kept $\sim\Delta^4$. The use of the second-order FD method leads to the overall convergence rate of order of Δ due to the discontinuity of the potential.

In order to choose the appropriate numerical scheme, we compared the exciton ground state energy, E_x, calculated using the second-order FDs and fourth-order FDs (A1) and (A2) in Eq. (5). The convergence of the exciton ground state energy as a function of the square of the grid step, Δ^2, is presented in Fig. 9 for AlGaAs and QW widths $L = 5$, 100 nm. Although both schemes provide convergence to almost the same values of energy as $\Delta^2 \to 0$, the rate of convergence is different. For the energy obtained using the second-order FD, the rate of convergence considerably depends on the width of QW. For QWs of small widths (of order of the Bohr radius a_B), the linear convergence (with respect to Δ^2) is observed for both schemes, whereas for wide QWs the second-order scheme gives a nonlinear convergence rate as $\Delta^2 \to 0$. The nonlinear convergence rate for the second-order scheme with respect to Δ is also obtained. The latter means that this scheme does not allow one to achieve the convergence region where the numerical solution would have the uncertainty proportional to Δ. The energy obtained using the fourth-order FD shows the linear dependence on Δ^2 for the whole range of the studied QW widths. It means

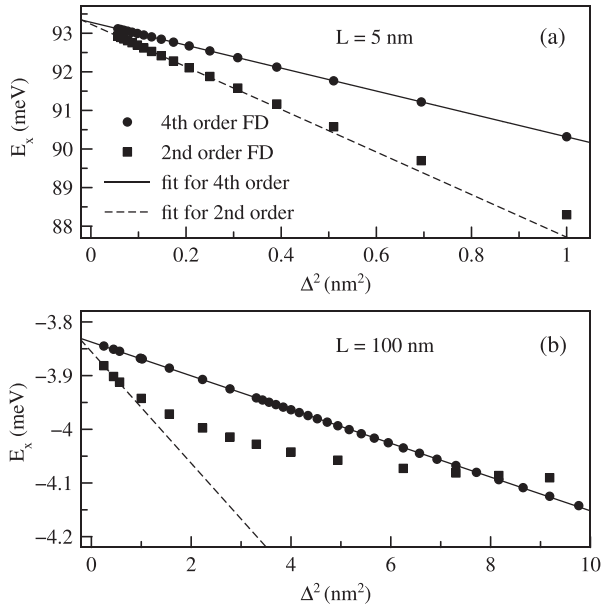

FIG. 9. The dependence of the exciton ground state energy, E_x, on the square of the grid step, Δ^2, (a) for QW width $L = 5$ nm and (b) for QW width $L = 100$ nm. The solid points are the calculated values of the energy. The solid lines indicate fits of the energy calculated using the fourth-order FD scheme, whereas the dashed lines show possible extrapolations of the data obtained using the second-order FD scheme.

that the use of the fourth-order scheme allows one to reach the convergence region where the accuracy of the numerical solution is of order of Δ^2. As a result, we employed the fourth-order FDs, performed a least square fit of the calculated energy, and extrapolated it to $\Delta = 0$. The uncertainties estimated from the least square fit are quite small. Thus, we obtained the precise exciton ground state energy. The typical grid step reached in the calculations with the QW widths comparable with a_B is $\Delta = 0.25$ nm, whereas for wide QWs, the achieved grid step $\Delta = 0.5$ nm.

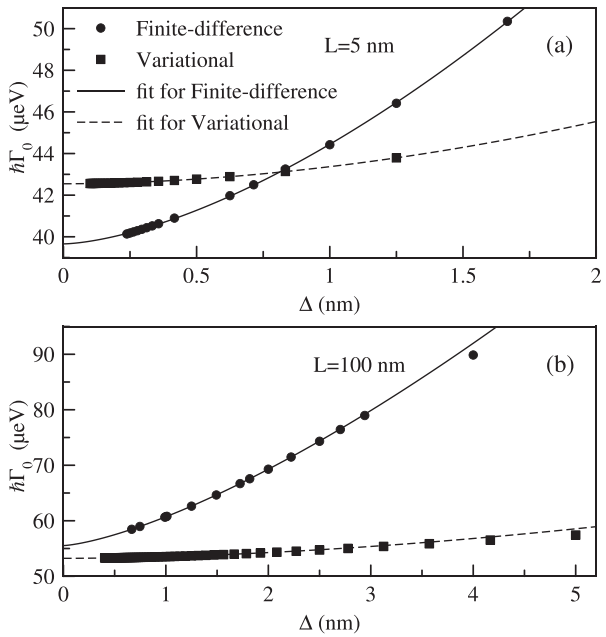

FIG. 10. The dependence of the radiative decay rate, $\hbar\Gamma_0$, on the grid step, Δ, (a) for QW width $L = 5$ nm and (b) for QW width $L = 100$ nm. The solid points are the calculated values of $\hbar\Gamma_0$. The solid curves indicate fits of the decay rates calculated using the FD numerical solution, whereas the dashed curves show fits of the values obtained using the variational approach.

For the radiative decay rate in energy units, $\hbar\Gamma_0$, calculated using the ground state wave function obtained from the finite-difference solution, the convergence is not so precise. The examples of the convergence rate for direct calculation of $\hbar\Gamma_0$ are shown in Fig. 10. For different QW widths, the convergence rate is different. We fitted the convergence rate as $\Delta \to 0$ by the function $\hbar\Gamma_0(\Delta) = a\Delta^b + c$, where a, $1 < b < 2$, and c are fitted parameters. The uncertainty was estimated as a discrepancy of the calculated and extrapolated values. This discrepancy is smaller for narrow QWs than for the wide QWs. As a result, the uncertainty of our extrapolation for obtaining the precise radiative decay rate was estimated as 1.5 μeV for QW width $L < 50$ nm and 3 μeV for wider QWs. For the variational calculations, the convergence rate is good enough for precise extrapolation of the radiative decay rate. This fact is also illustrated in Fig. 10.

[1]W. W. Chow and S. W. Koch, *Semiconductor-Laser Fundamentals* (Springer, 1999).
[2]E. F. Schubert, *Light-Emitting Diodes* (Cambridge University Press, Cambridge, 2006).
[3]V. K. Khanna, *Fundamentals of Solid State Lighting: LEDs, OLEDs, and Their Application in Illumination and Displays* (CRC Press, 2014).
[4]P. Andreakou, S. V. Poltavtsev, J. R. Leonard, E. V. Calman, M. Remeika, Y. Y. Kuznetsova, L. V. Butov, J. Wilkes, M. Hanson, and A. C. Gossard, Appl. Phys. Lett. **104**, 091101 (2014).
[5]H. Flayac and I. G. Savenko, Appl. Phys. Lett. **103**, 201105 (2013).
[6]F. Marsault, H. S. Nguyen, D. Tanese, A. Lemaître, E. Galopin, I. Sagnes, A. Amo, and J. Bloch, Appl. Phys. Lett. **107**, 201115 (2015).
[7]C. Antón, T. C. H. Liew, G. Tosi, M. D. Martín, T. Gao, Z. Hatzopoulos, P. S. Eldridge, P. G. Savvidis, and L. Viña, Appl. Phys. Lett. **101**, 261116 (2012).
[8]E. F. Gross and N. A. Karryev, Dokl. Acad. Sci. USSR **84**, 261 (1952); E. F. Gross and N. A. Karryev *ibid.* **84**, 471 (1952).
[9]G. Bastard, E. E. Mendez, L. L. Chang, and L. Esaki, Phys. Rev. B **26**, 1974 (1982).
[10]J. H. Davies, *The Physics of Low-Dimensional Semiconductors* (Cambridge University Press, Cambridge, 1998).
[11]E. L. Ivchenko, *Optical Spectroscopy of Semiconductor Nanostructures* (Alpha Science, Harrow, 2005).
[12]S. W. Koch, M. Kira, G. Khitrova, and H. M. Gibbs, Nat. Mater. **5**, 523 (2006).
[13]R. P. Seisyan, Semicond. Sci. Technol. **27**, 053001 (2012).
[14]M. Glauser, C. Mounir, G. Rossbach, E. Feltin, J.-F. Carlin, R. Butté, and N. Grandjean, J. Appl. Phys. **115**, 233511 (2014).
[15]Ü. Özgür, Ya. I. Alivov, C. Liu, A. Teke, M. A. Reshchikov, S. Doğan, V. Avrutin, S.-J. Cho, and H. Morkoç, J. Appl. Phys. **98**, 041301 (2005).
[16]R. Knox, *Theory of Excitons* (Academic Press, New York, 1963).
[17]E. I. Rashba and G. E. Gurgenishvilli, Sov. Phys. Solid State **4**, 759 (1962) [Fiz. Tverd. Tela **4**, 1029 (1962)].
[18]A. V. Kavokin, Phys. Rev. B **50**, 8000 (1994).
[19]J. P. Prineas, C. Ell, E. S. Lee, G. Khitrova, H. M. Gibbs, and S. W. Koch, Phys. Rev. B **61**, 13863 (2000).
[20]T. Kazimierczuk, D. Fröhlich, S. Scheel, H. Stolz, and M. Bayer, Nature **514**, 343 (2014).
[21]A. V. Kavokin, J. J. Baumberg, G. Malpuech, and F. P. Laussy, *Microcavities* (Oxford University Press, Oxford, 2007).
[22]H. M. Gibbs, G. Khitrova, and S. W. Koch, Nat. Photonics **5**, 273 (2011).
[23]V. Srinivas, Y. J. Chen, and C. Wood, Phys. Rev. B **48**, 12300 (1993).
[24]S. V. Poltavtsev and B. V. Stroganov, Phys. Solid State **52**, 1899 (2010) [Fiz. Tverd. Tela **52**, 1769 (2010)].
[25]S. V. Poltavtsev, Yu. P. Efimov, Yu. K. Dolgikh, S. A. Eliseev, V. V. Petrov, and V. V. Ovsyankin, Solid State Commun. **199**, 47 (2014). In this paper, a quantity $\hbar\Gamma_0$ denotes the full width of the radiative broadening for exciton resonances and, therefore, it is twice larger than that defined in our work.

[26]J. Shah, *Ultrafast Spectroscopy of Semiconductors and Semiconductor Nanostructures* (Springer, Heidelberg, 1999).
[27]D. Bajoni, P. Senellart, M. Perrin, A. Lemaître, B. Sermage, and J. Bloch, Phys. Status Solidi B **243**, 2384 (2006).
[28]M. T. Portella-Oberli, J. Berney, L. Kappei, F. Morier-Genoud, J. Szczytko, and B. Deveaud-Plédran, Phys. Rev. Lett. **102**, 096402 (2009).
[29]R. Singh, T. M. Autry, G. Nardin, G. Moody, H. Li, K. Pierz, M. Bieler, and S. T. Cundiff, Phys. Rev. B **88**, 045304 (2013).
[30]A. Baldereschi and N. O. Lipari, Phys. Rev. B **3**, 439 (1971).
[31]J. M. Luttinger, Phys. Rev. **102**, 1030 (1956).
[32]R. C. Miller, D. A. Kleinman, W. T. Tsang, and A. C. Gossard, Phys. Rev. B **24**, 1134 (1981).
[33]R. L. Greene, K. K. Bajaj, and D. E. Phelps, Phys. Rev. B **29**, 1807 (1984).
[34]J. Lee, H. N. Spector, and P. Melman, J. Appl. Phys. **58**, 1893 (1985).
[35]R. P. Leavitt and J. W. Little, Phys. Rev. B **42**, 11774 (1990).
[36]H. Mathieu, P. Lefebvre, and P. Christol, J. Appl. Phys. **72**, 300 (1992).
[37]L. Hrivnák, J. Appl. Phys. **72**, 3218 (1992).
[38]B. Gerlach, J. Wüsthoff, M. O. Dzero, and M. A. Smondyrev, Phys. Rev. B **58**, 10568 (1998).
[39]K. Sivalertporn, L. Mouchliadis, A. L. Ivanov, R. Philp, and E. A. Muljarov, Phys. Rev. B **85**, 045207 (2012).
[40]S. K. Lyo and W. Pan, J. Appl. Phys. **118**, 195705 (2015).
[41]J. W. Brown and H. N. Spector, J. Appl. Phys. **59**, 1179 (1986).
[42]R. H. Yan, F. Laruelle, and L. A. Coldren, Appl. Phys. Lett. **55**, 2002 (1989).
[43]D. B. T. Thoai, R. Zimmermann, M. Grundmann, and D. Bimberg, Phys. Rev. B **42**, 5906(R) (1990).
[44]C. Huo, B.-Y. Gu, and L. Gu, J. Appl. Phys. **70**, 4357 (1991).
[45]C. P. Hilton, W. E. Hagston, and J. E. Nicholls, J. Phys. A: Math. Gen. **25**, 2395 (1992).
[46]P. Bigenwald and B. Gil, Solid State Commun. **91**, 33 (1994).
[47]T. Piorek, W. E. Hagston, and P. Harrison, Phys. Rev. B **52**, 14111 (1995).
[48]A. Montes, C. A. Duque, and N. Porras-Montenegro, J. Appl. Phys. **81**, 7890 (1997).
[49]M. Bouhassoune, R. Charrour, M. Fliyou, D. Bria, and A. Nougaoui, J. Appl. Phys. **91**, 232 (2002).
[50]L. I. Deych and I. V. Ponomarev, Phys. Rev. B **71**, 035342 (2005).
[51]L. C. Andreani and A. Pasquarello, Phys. Rev. B **42**, 8928 (1990).
[52]L. C. Andreani, Solid State Commun. **77**, 641 (1991).
[53]D. S. Citrin, Phys. Rev. B **47**, 3832 (1993).
[54]L. C. Andreani, R. C. Iotti, R. Schwabe, F. Pietag, V. Gottschalch, A. Bitz, and J.-L. Staehli, Physica E **2**, 151 (1998).
[55]R. C. Iotti and L. C. Andreani, Phys. Rev. B **56**, 3922 (1997).
[56]A. D'Andrea, N. Tomassini, L. Ferrari, M. Righini, S. Selci, M. R. Bruni, D. Schiumarini, and M. G. Simeone, J. Appl. Phys. **83**, 7920 (1998).
[57]B. Deveaud, F. Clérot, N. Roy, K. Satzke, B. Sermage, and D. S. Katzer, Phys. Rev. Lett. **67**, 2355 (1991).
[58]B. Zhang, S. S. Kano, Y. Shiraki, and R. Ito, Phys. Rev. B **50**, 7499 (1994).
[59]V. Voliotis, R. Grousson, P. Lavallard, and R. Planel, Phys. Rev. B **52**, 10725 (1995).
[60]B. Deveaud, L. Kappei, J. Berney, F. Morier-Genoud, M. T. Portella-Oberli, J. Szczytko, and C. Piermarocchi, Chem. Phys. **318**, 104 (2005).
[61]A. V. Trifonov, S. N. Korotan, A. S. Kurdyubov, I. Ya. Gerlovin, I. V. Ignatiev, Yu. P. Efimov, S. A. Eliseev, V. V. Petrov, Yu. K. Dolgikh, V. V. Ovsyankin, and A. V. Kavokin, Phys. Rev. B **91**, 115307 (2015).
[62]V. V. Belykh and M. V. Kochiev, Phys. Rev. B **92**, 045307 (2015).
[63]D. K. Loginov, A. V. Trifonov, and I. V. Ignatiev, Phys. Rev. B **90**, 075306 (2014).
[64]M. Altarelli and N. O. Lipari, Phys. Rev. B **9**, 1733 (1974).
[65]A. Siarkos, E. Runge, and R. Zimmermann, Phys. Rev. B **61**, 10854 (2000).
[66]A. L. C. Triques and J. A. Brum, Phys. Rev. B **56**, 2094 (1997).
[67]L. D. Landau and E. M. Lifshits, *Quantum Mechanics. Nonrelativistic Theory* (Nauka, Moscow, 2004).
[68]B. R. Johnson, Phys. Rev. A **24**, 2339 (1981).
[69]D. C. Sorensen, R. B. Lehoucq, and P. Vu, *ARPACK: An Implementation of the Implicitly Restarted Arnoldi Iteration that Computes Some of the Eigenvalues and Eigenvectors of a Large Sparse matrix* (Rice University, 1995).
[70]P. S. Grigoryev, A. S. Kurdyubov, M. S. Kuznetsova, Yu. P. Efimov, S. A. Eliseev, V. V. Petrov, V. A. Lovtcius, P. Yu. Shapochkin, and I. V. Ignatiev, "Excitons in asymmetric quantum wells," e-print arXiv:1602.03720.
[71]D. Schiumarini, N. Tomassini, L. Pilozzi, and A. D'Andrea, Phys. Rev. B **82**, 075303 (2010).
[72]C. G. Van de Walle, Phys. Rev. B **39**, 1871 (1989).
[73]I. Vurgaftman, J. R. Meyer, and L. R. Ram-Mohan, J. Appl. Phys. **89**, 5815 (2001).
[74]M. Kumagai and T. Takagahara, Phys. Rev. B **40**, 12359 (1989).
[75]A. D'Andrea and R. Del Sole, Phys. Rev. B **25**, 3714 (1982).
[76]A. Tredicucci, Y. Chen, F. Bassani, J. Massies, C. Deparis, and G. Neu, Phys. Rev. B **47**, 10348 (1993).
[77]E. V. Ubyivovk, D. K. Loginov, I. Ya. Gerlovin, Yu. K. Dolgikh, Yu. P. Efimov, S. A. Eliseev, V. V. Petrov, O. F. Vyvenko, A. A. Sitnikova, and D. A. Kirilenko, Phys. Solid State **51**, 1929 (2009) [Fiz. Tverd. Tela **51**, 1818 (2009)].
[78]K. Muraki, S. Fukatsu, Y. Shiraki, and R. Ito, Appl. Phys. Lett. **61**, 557 (1992).
[79]L.-W. Wang and A. Zunger, Phys. Rev. B **54**, 11417 (1996).
[80]A. Di Carlo, Semicond. Sci. Technol. **18**, R1 (2003).
[81]G. F. Glinskii, V. A. Lakisov, A. G. Dolmatov, and K. O. Kravchenko, Nanotechnology **11**, 233 (2000).
[82]M. M. Voronov, E. L. Ivchenko, V. A. Kosobukin, and A. N. Poddubny, Phys. Solid State **49**, 1792 (2007) [Fiz. Tv. Tela **49**, 1709 (2007)].
[83]V. A. Kiselev, I. V. Makarenko, B. S. Razbirin, and I. N. Ural'tsev, Sov. Phys. Solid State **19**, 1374 (1977) [Fiz. Tverd. Tela (Leningrad) **19**, 2348 (1977)].
[84]L. Collatz, *The Numerical Treatment of Differential Equations* (Springer, New York, 1966).
[85]G. I. Marchuk and V. V. Shaidurov, *Difference Methods and Their Extrapolations* (Springer, Berlin, 1983).
[86]A. A. Samarskii, *The Theory of Difference Schemes* (Nauka, Moscow, 1989).